IDEI 80 Scientific report january-december 2013

Phase III Comparated experiments regarding the laser pyrolysis synthesis of the TiO_2 nanoparticles covered with siloxane polymers: complex chacaterizations.

In the literature there are few studies of the effect of polymeric dispersants adsorbed on the surface of TiO2 nanoparticles and especially those of change using policarbosiloxanic polymers are missing. Instead, were tested on foil packaging plastic food ("food packaging") in which dispersed TiO2 nanoparticles inhibit / destroy bacteria by photochemical sterilization

1.1. Synthesis by laser pyrolysis of TiO2 nanoparticles coated by carbosilanic polymer (HDMSO precursor)

As we have reported in previous phases, the laser pyrolysis experimental installation used by us, precursors and other auxiliary gas (confinement, dilution, oxidant sensitivity) are inserted through an injector consists of three cylindrical tubes (Figure 1) located about 7 mm below the infrared beam emitted by the CO2 laser, narrowed in this area to a diameter of 5 mm with a ZnSe lens. Another stream of gas introduced into the reaction chamber is the protection of windows, each 850 sccm argon, serving to prevent any particles to attach to them, and which could result in local absorption of laser beam to create incandescent points resulted in the destruction of their windows.

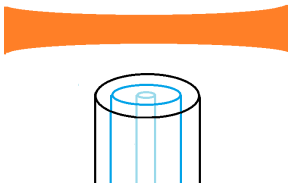

Fig.1 Schematic representation of the injector and the laser beam
(in reality invisible to the naked eye)

At this stage, we performed several experiments, nine of them are presented here, two of which were used as references (TLOP01 and TLOP04), meaning that no silicon precursor was introduced at all. And gas flow rates introduced are summarized in Table 1

Exp.	**Gas flow by nozzle**										
	Central [sccm]				**Intermedaite [sccm]**						**External [sccm]**
	Air>	**C_2H_4>**	**Add.**	**C_2H_4>**	**Air>**	**C_2H_4>**	**Add.**	**C_2H_4>**	**Ar**	**C_2H_4**	**Ar**

	$TiCl_4$	$TiCl_4$	Air	$[(CH_3)_3Si]_2O$	$TiCl_4$	$TiCl_4$	Air	$[(CH_3)_3Si]_2O$			
TLOP9				**20**	**200**	**60**	**400**				**1700**
TLOP10				**20**	**100**	**30**	**200**				**1500**
TLOP11			**40**	**20**	**110**	**20**	**450**				**1700**
TLOP04	**200**	**60**					**200**			**20**	**1700**
TLOP01	**200**	**60**							**1700**		
TLOP5	**200**	**60**						**20**	**200**		**1700**
TLOP6	**200**	**60**					**200**	**20**			**1700**
TLOP7	**200**	**60**					**300**	**20**			**1700**
TLOP8	**200**	**60**					**400**	**20**			**1700**

Table 1. Presentation of the gas / vapor flows introduced into the experiments

The difference between the two experiments is that the reference to TLOP 01 were used only two of the three nozzles, argon confinement being introduced through intermediate nozzle, while in the TLOP 04 20 sccm of ethylene and another of 200 sccm of air was introduced through the intermediate, analogous to the one used in the experiment TLOP6.

Note that for entraining the $TiCl_4$ vapors we used a mixture of air and ethylene. Also ethylene was used for bubbling and training hexamethyldisiloxane vapors $[(CH_3)_3Si]_2O$, denoted HMDSO. Pressure of 550 mbar was used to facilitate the involvement of as much quantity of titanium and silicon precursors at room temperature from those two bubblers. Maintaining constant pressure in the reaction chamber was achieved by equalizing the input streams at the output with an electro valve fitted with a clamshell that can adjust the gas flow exiting the filter chamber, located above the reaction chamber.
The laser power was 350 W, which means a laser power density of about 1780 W/cm2. This amount of power density was chosen to simultaneously fulfill two conditions: first must be high enough to initiate a stable laser pyrolysis flame, on the other side does not have to be too high because it would enhance the decomposition of ethylene to carbon and the formation of titanium dioxide rutile phase in a greater proportion to its most active phase, anatase.
In the first set of experiments, TLOP 5 .... 8, the Ti precursor is introduced through the central nozzle and Si precursor through the intermediate nozzle, varying the airflow only additional intermediate nozzle from zero to 400 sccm (in TLOP5 instead of air introduced an even flow of Ar to keep the same speed gas from TLOP6 experiment, and to limit oxidation of HMDSO in order to obtain polymers mainly carbosiloxanes instead of silica).
In the second set of experiments TLOP 9 ... 11, the position of the precursors flows was reversed, so that HMDSO is introduced through the central nozzle and $TiCl_4$ through the intermediate nozzle reducing both the ethylene flow and that the air (vapor carriers of TiCl4), since ethylene bearing HMDSO flow was maintained constant, the same as in the first series of experiments, 20

sccm. The last two experiments, although the total amount of $TiCl_4$ involved was the same, we used 100 sccm air and 30 sccm C_2H_4 (TLOP10) or 120 sccm air and 20 sccm C_2H_4 (TLOP11) ethylene flow to TLOP11 being lowest (and the air is greater) was intended to result in less carbon. Thus, in the TLOP11experiment was much larger amount of air, leading to a total of 40 + 110 + 450 = 700 sccm to a total of 100 + 200 = 300 sccm for TLOP10 and finally to a total of 200 + 400 = 600 sccm for TLOP9 experiment. Due to tje lower Ti precursor amount introduced in the last two experiments (TLOP 10 and 11), it is aspected that the atomic percent of Ti in the corresponding powders to be lower. Other difference between the two series of experiments arose from the difference between the cross-sectional area of inner nozzle and the concentric nozzle. Thus at equal flow through those nozzles, the central flow velocity will be 10 times grater and the time of the species passing through the laser beam will be considerably lower

Fig.2. Photographies of laser oxidative pyrolysis flames from $TiCl_4$, HMDSO and air mixtures

One can see from the fig.2 that the laser oxidative flames extend upstream, outside from the laser beam. This behavior is due to the ethylene burning in air. TLOP-7 and TLOP11 flames also extend downward (again outside ftom IR lase beam) very near to the glass injector end due to the higher amount of oxidant available.

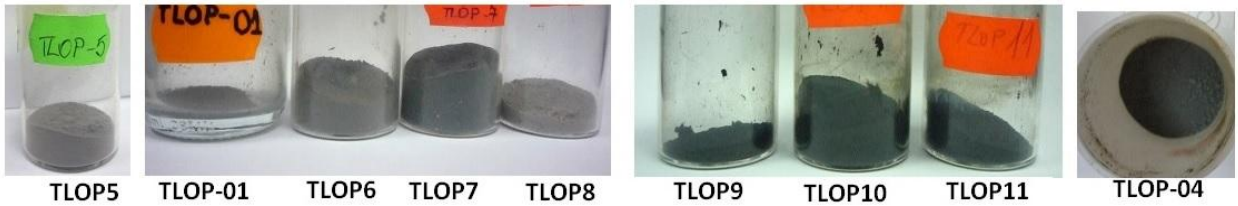

Fig.3. Photographies of the as-obtained raw powders

The grey color of powders is due to their carbon content provided by ethylene decomposition in the presence of insufficient amount of oxidant. The dark blue color can be explained by the supplementary presence of Ti^{3+} ions as suboxides (TiO_{2-x})

Some of the principal chemical reactions involved in our experiments can be summarized as following: $TiCl_4 + \mathbf{O_2} \rightarrow TiO_2 + 2\ Cl_2$ and $C_6H_{18}Si_2O + \mathbf{12\ O_2} \rightarrow 2\ SiO_2 + 6\ CO_2 + 9\ H_2O$
$C_2H_4 + \mathbf{3\ O_2} \rightarrow 2\ CO_2 + 2\ H_2O$ for stoechiometric amount of oxygen; As discussed, we must account for the reactions in an insufficient oxidant conditions:
$C_2H_4 + \mathbf{2\ O_2} \rightarrow 2CO + 2\ H_2O$ and $C_2H_4 + \mathbf{O_2} \rightarrow 2\ CO + 2\ H_2$ or even in the absence of O2:
$C_2H_4 \rightarrow C_2H_2 + H_2$; $C_2H_2 \rightarrow 2C + H_2$; $C_2H_4 \rightarrow 2\ C + 2\ H_2$ and $C_6H_{18}Si_2O \rightarrow (C_xH_ySi_zO_w) + n\ CH_4 + m\ H_2$

The amount of vapors of Ti and Si precursors depend of the pressure in the bublers (approximated as being the same with the working pressure in the reaction chamber) and on the carring gas flows through the volatile liquids (ethilene/air).

In the TLOP8 experiment a tronconical deposit was also formed on the central nozzle rim. This deposit was also collected and shows a silicon and titanium segregation (by EDX elemental evaluation). This can be explained bai the incomplete mixing of TICl4 flow from the center and HMDSO from the annular co-flow. SEM image (fig4) also show the more compact morphology from this special deposit. The fine morphology of the resulted powders is visible also in the other SEM images from fig. 4 and 5.

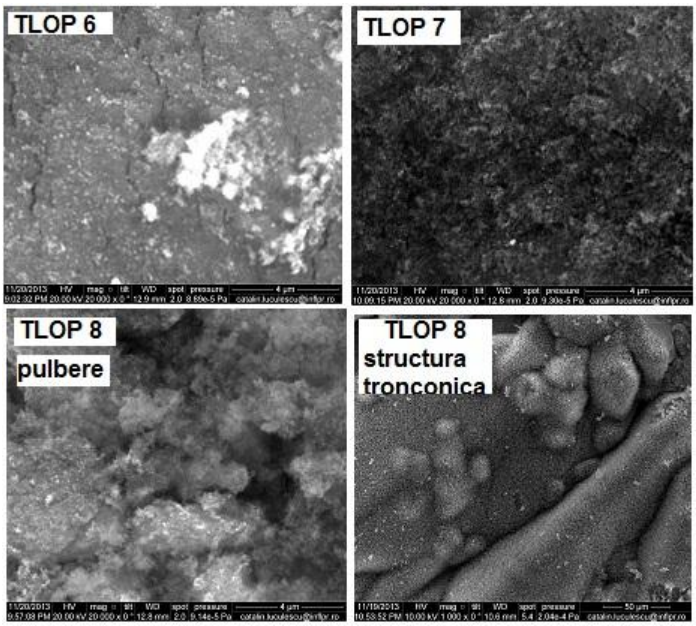

Fig.4 SEM images from nanopowders resulted in TLOP 6.7 and 8 experiments

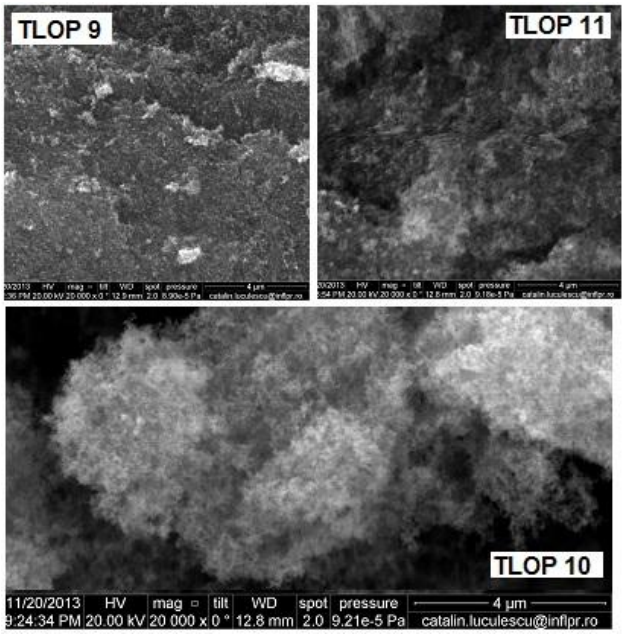

Fig,5. SEM images from nanopowders resulted in TLOP 9,10 and 11 experiments

The TLOP11 SEM image (fig.5, down) withesses also the nanometric, porous morphology specific to the laser pyrolysis sinthesized powders

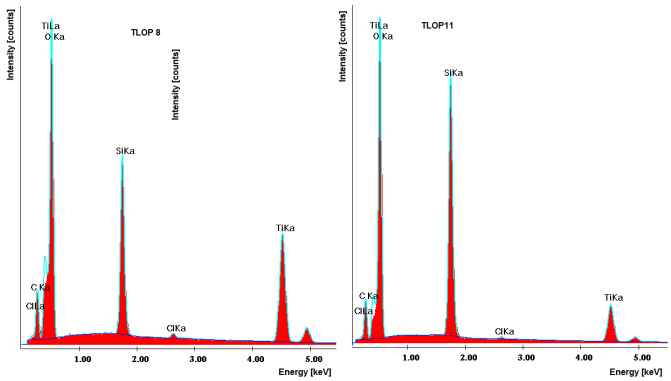

Fig,6 EDX spectra from TLOP8 and 11 nanopowders

Sample	Ti [at%]	Si [at%]	O [at%]	C [at%]	Cl [at%]	Ti/Si atomic ratio
TLOP 01	21.23	-	59.68	18.85	0.24	-
TLOP 04	14.61	-	60.72	24.31	0.36	-
TLOP5	19.46	5.80	47.38	27.21	0.15	**3.35**
TLOP6	14.24	5.99	54.95	24.68	0.14	**2.38**
TLOP7	16.95	8.92	54.12	19.86	0.14	**1.90**
TLOP8	19.22	9.79	55.54	15.12	0.33	**1.96**
TLOP9	15.16	7.77	44.60	32.18	0.29	**1.95**
TLOP10	8.27	11.80	37.19	42.28	0.46	**0.7**
TLOP11	9.09	18.08	52.62	20	0.21	**0.5**

Table 2. Elemental composition (atomic percents) from TLOP samples by EDX analyses

The EDX analises can't discriminate the bonding and phases but can allow an estimation of the elemental percent of Ti, S, C and O atoms (see Table 2). Generally, the lowe percent of air introduced results in powders with a higher carbon content as expected. Also the ration betweenj titanium sna silicon atoms can be related with the ratio of the precursors, knowing that from one mole of $TiCl_4$ results one mole of titania wherea from one mole of HMDSO results two moles of silica. Small amount of chlorine is retaining inther raw powders from the TiCl4 precursor. TLOP10 sample resulting from the most oxigen-deficient mixture (minimum amount of air from all the experiments) has the highest atomic percent of carbon = around 40%

The presence of anatase and rutile titania phases is visible in the X-ray diffractograms from fig. 7 and 8. A very broad peak (2θ=20..26°) visible as a baseline bump in TLOP10 sample is due to the amorphous/disrdered carbon mixed with amorphous silica. The TLOP11 sample presents a similar yet smaller peak - in this case the amorphous silica seems to be the main surse

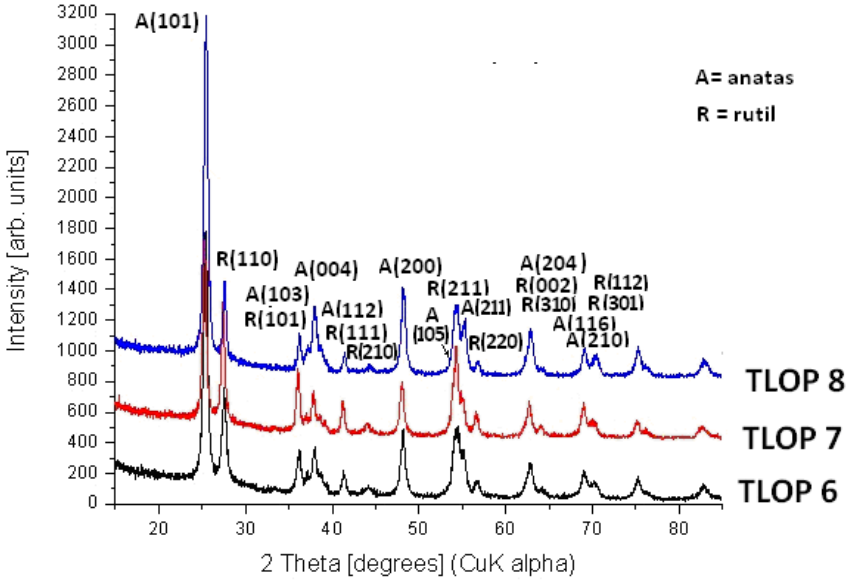

Fig.7 X-ray Superposed diffractograms of eaw TLOP 6, 7 si 8 nanopowders

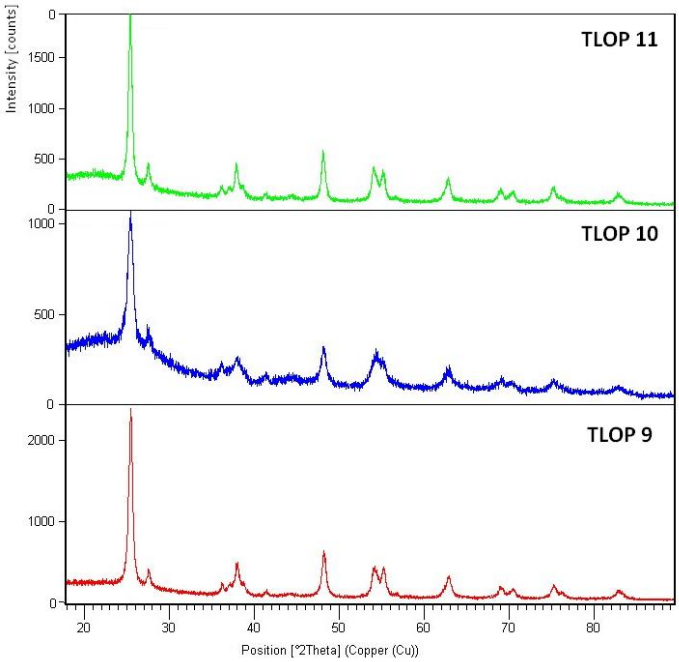

Fig.8 X-ray Superposed diffractograms of raw TLOP 9, 10 and 11 nanopowders

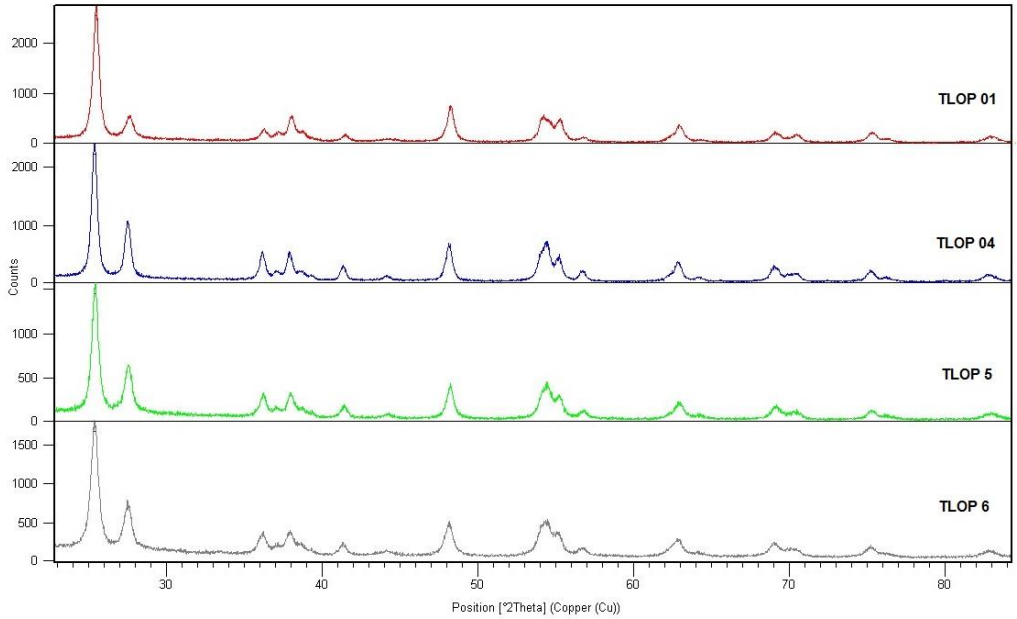

Fig.9 X-ray Superposed diffractograms of raw **TLOP 01, 04, 5 si 6 samples**

No signature of titanium suboxides can be seen in the diffractograms from fig. 7, 8 and 9. It is very possibe that these compounds to be amorphous and to be integrated in the background noise

Sample	Anatase mean crystallite size [nm]	Rutile mean crystallite size [nm]	%Anatas/ /[%Anatas + %Rutil]	%Rutil/ /[%Anatas + %Rutil]
TLOP 01	22	17	83.3	17.7
TLOP 04	24	23	65.8	34.2
TLOP 5	19	15	69.04	30.96
TLOP 6	17	15	39.36	60.64
TLOP 7	18	19	53.55	46.45
TLOP 8	18	24	78	22
TLOP 9	15	15	90.52	9.48
TLOP 10	11	6	85.06	14.94
TLOP 11	21	18	86.69	13.31

Table 3. Crystallite meand sized (anatase and rutile) and their ratio in TLOP nanopowders

A very broad peak centered around 2θ~26° can also be found in various disordered carbonaceous materials such as those obtained from incomplete (incipient) carbonization of organic substances

such as saccharose dehydration/carbonization with concentrated sulfuric acid or form pyrolysis of various wooden products [20], [21]. As can be seen from the Table 3, the samples obtained when HMDSO was introduced through the central nozzle show the higher anatase content 85-90% .

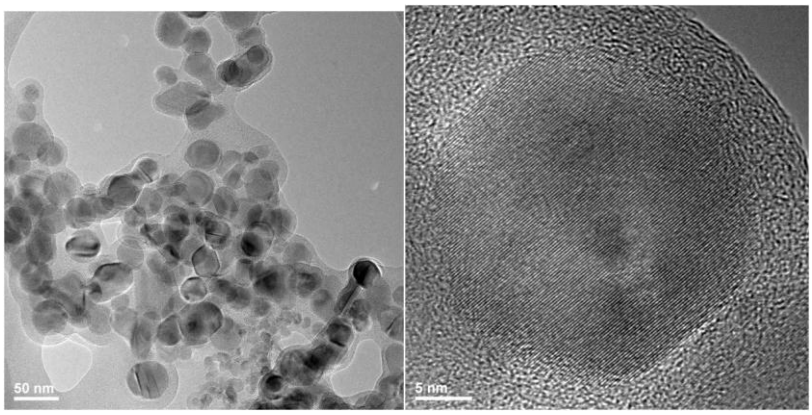

Fig.10 TEM image (left)and HRTEM (right) from TLOP6 sample

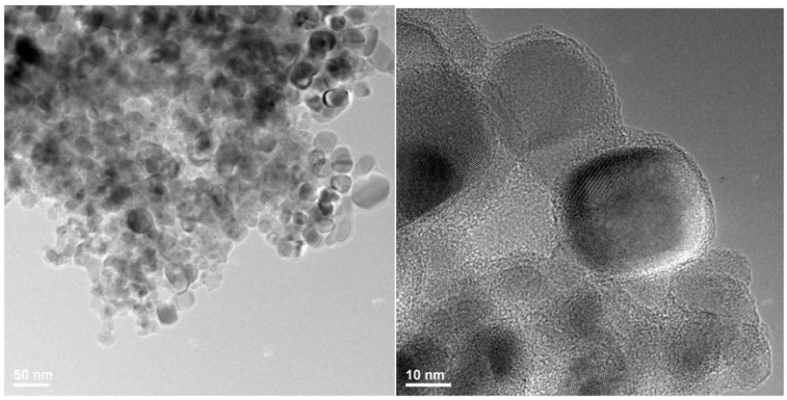

Fig.11 TEM image (left)and HRTEM (right) from TLOP7 sample

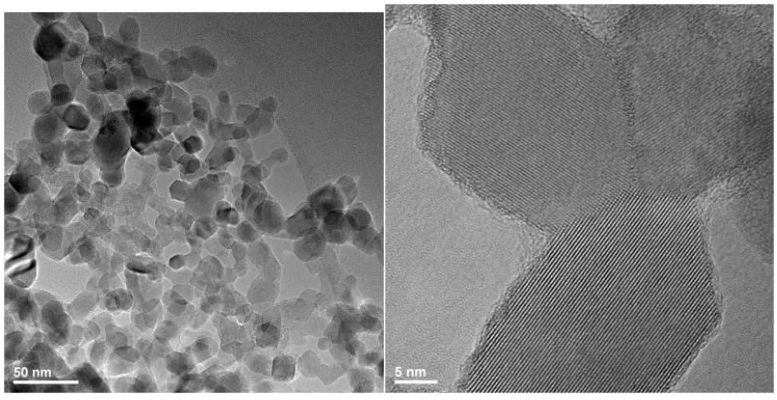

Fig.12 TEM image (left)and HRTEM (right) from TLOP8 sample

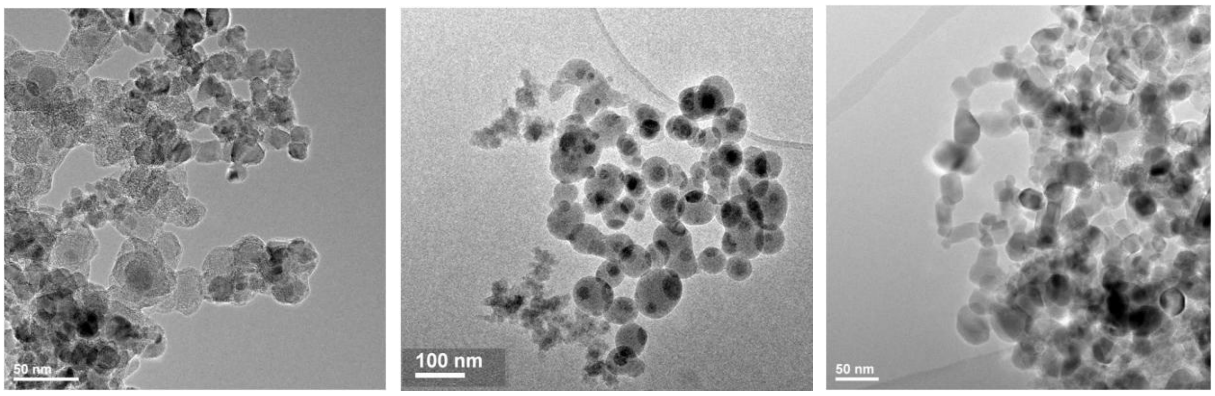

Fig.13 TEM Imagies from TLPO 9(left), TLOP10 (center) and TLOP11 (right) nanopowders

TEM images from fig.10-13 show chained/aggregated nanoparticles some with a core-shell morphology. Higher magnifivationn TEM from fig 10 and 11 clearly show a crystalline nanoparticles surrounded br a disordered/amorphous shell than must consis of carbon and/or silica. Generally the size of nanoparticles are under 100 nm, with many having sizes around 10-30 nm, depending of sample.

Generally, the UV-VIS absorbamce spectra from the ultrasonicated diluted suspensions from the raw TLOP nanopowders (presented in fig.14 and 13) show the typical high absorption behavior in ultraviolet zone, extending for some to the 400-500 nm visible region

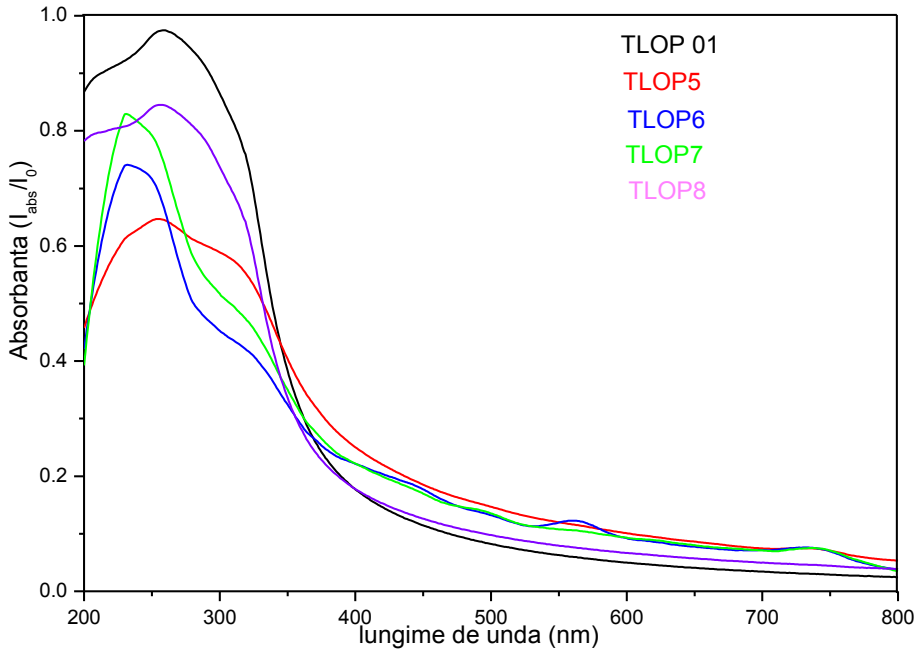

Fig.14 UV-VIZ superposed spectra from TLOP01, si TLOP 4, 5, 6, 7 and 8 nanoparticles as aqueous ultrasonicated suspensions

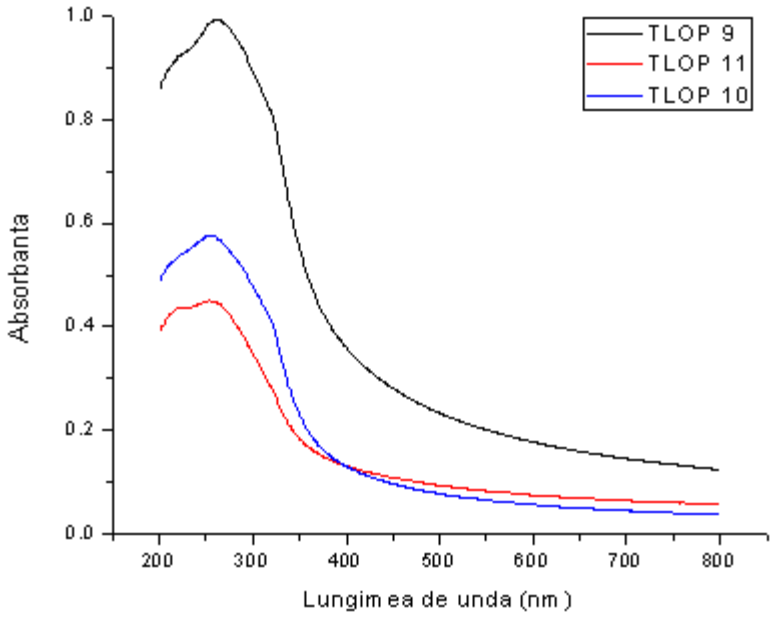

Fig.15 UV-VIZ superposed spectra from TLOP01, si TLOP 9,10 and 11 nanoparticles as aqueous ultrasonicated suspensions

Bibliography

[1] H. Zhang et al., *Environ. Sci. Technol.* **42**, 3803 (2008)
[2] S. Abramson et al., *J. Nanopart. Res.,* **11**, 459 (2009)
[3] A. Kanta et al., *Colloids and Surfaces A* **92,** 1 (2007)
[4] J. Pola et al., *Appl. Organometal. Chem*. **19**, 1015 (2005)
[5] D. Kannaiyan et al., *Polymers* ***2,*** 490 (2010)
[6] A. Nilchi et al. *Mater. Sci. Appl.* **2**, 476 (2011)
[7] S. Ramesh et al., *Nanoscale Res. Lett.* **7**, 350 (2012)
[8] V.M. Gun'ko et al., *Powder Technol*. **164**, 153 (2006)
[9] S.H. Ehrman et al., *J. Mater. Res.* **14**, 4551 (1999)
[10] S.H. Jeon et al. *Appl. Chem* **10**, 364 (2006)
[11] B. Buesser, S.E. Pratsinis, *AIChE J*. 57, 3132 (2011)
[12] N.S. Subramanian et al., US Patent 2,00,627,303 (A1), 2006.
[13] M. Scarisoreanu et. al., *Appl. Surf. Sci*. **278**, 295 (2013)
[14] A.K. Bhanwala et al., *Aerosol Sci.* **40**, 720 (2009)
[15] H. Maskrot et al., *J. Nanop. Res.* **8**, 351 (2006)
[16] S.H. Ehrman et al., *J. Aerosol Sci.* **29**, 687 (1998)
[17] R.H. West et al., *J. Phys. Chem. A* **111**, 3560 (2007)
[18] J.H. Kim et al., *J. Sol-Gel Sci. Technol.* **32**, 31 (2004)
[19] D. Hoebbel et al., *J. Sol-Gel Sci. Technol.* **13**, 37 (1998)

[20] M.W. Awitdrus et al, *Sains Malaysiana* **39**, 83 (2010)
[21] P. Gao et al., *Ceramics Int.* **34**, 1975 (2008)
[22] S. Music et al., *Braz. J. Chem. Eng.* **28**, 89 (2011)

Activitate manageriala, diseminare, editare

Poster V Symposia "Laser materials interactions for micro and nano applications" - E-MRS Spring Meeting, , Strasbourg, Franta 27-31 mai 2013 "**Recent progress in the synthesis of magnetic titania/iron-based composite nanoparticles manufactured by laser pyrolysis**: autori R. Alexandrescu, M. Scarisoreanu, I. Morjan, I.P. Morjan, F. Dumitrache, ***C.T. Fleaca***, R. Birjega, G. Filoti, V. Kuncser, V. Danciu

- Scientific article "**Recent progress in the synthesis of magnetic titania/iron-based composite nanoparticles manufactured by laser pyrolysis**" *Appl. Surf. Sci.,* in press (in curs de aparitie) 2013 http://dx.doi.org/10.1016/j.apsusc.2013.10.138 , autori ***C.T. Fleaca***, M. Scarisoreanu, I. Morjan, R. Alexandrescu, F. Dumitrache, C. Luculescu, I.P. Morjan, R. Birjega, A.-M. Niculescu, G. Filoti, V. Kuncser, E. Vasile, V. Danciu, M. Popa

03.12.2013

Project Director, Dr. Claudiu Fleaca